Photochemistry and Photobiology, 2015, 91: 1219–1230

Impact of Substituents in Tumor Uptake and Fluorescence Imaging Ability of Near-Infrared Cyanine-like Dyes

Nayan J. Patel[1,2], Ethirajan Manivannan[2], Penny Joshi[2], Tymish J. Ohulchanskyy[3], Roger R. Nani[4], Martin J. Schnermann[4] and Ravindra K. Pandey[1,2]*

[1]Department of Molecular Pharmacology and Cancer Therapeutics, Cell Stress Biology Roswell Park Cancer Institute, Buffalo, NY
[2]PDT Center, Cell Stress Biology Roswell Park Cancer Institute, Buffalo, NY
[3]Institute for Lasers, Photonics and Biophotonics SUNY at Buffalo, Buffalo, NY
[4]Chemical Biology Laboratory, National Cancer Institute, National Institutes of Health, Frederick, MD

Received 18 January 2015, accepted 9 June 2015, DOI: 10.1111/php.12482

ABSTRACT

This report presents a simple strategy to introduce various functionalities in a cyanine dye (bis-indole-*N*-butylsulfonate-polymethine bearing a fused cyclic chloro-cyclohexene ring structure), and assess the impact of these substitutions in tumor uptake, retention and imaging. The results obtained from the structural activity relationship (SAR) study demonstrate that certain structural features introduced in the cyanine dye moiety make a remarkable difference in tumor avidity. Among the compounds investigated, the symmetrical CDs containing an amino-phenyl thioether group attached to a cyclohexene ring system and the two N-butyl linkers with terminal sulfonate groups in benzoindole moieties exhibited excellent tumor imaging ability in BALB/c mice bearing Colon26 tumors. Compared to indocyanine green (ICG), approved by FDA as a blood pooling agent, which has also been investigated for the use in tumor imaging, the modified CD selected on the basis of SAR study produced enhanced uptake and longer retention in tumor(s). A facile approach reported herein for introducing a variety of functionalities in tumor-avid CD provides an opportunity to create multi-imaging modality agent(s). Using a combination of mass spectrometry and absorbance techniques, the photobleaching of one of the CDs was analyzed and significant regioselective photooxidation was observed.

INTRODUCTION

Fluorescence optical imaging is a clinically underutilized imaging modality which in the last decade has seen rapid adoption in the field of oncology (1). Among the imaging modalities currently being used in tumor detection, none offer the versatility and promises of optical imaging. Historically, fluorescence imaging has almost exclusively been used in academic research for tracing cellular movements along with understanding expression levels and reaction rates of proteins (2). Fluorescence optical imaging works by first administering an exogenous biologically compatible fluorescent molecule (fluorophore) to the system and then using a light source to excite the fluorophore. Light of a longer wavelength is then emitted by the fluorophore and this emitted light can provide diagnostic information based on its localization or state. Unfortunately, limited penetration of light into tissue as a result of it attenuation due to scattering and absorption has been the major hindrance in the translation of this imaging technique into the clinic (3).

Imaging modalities such as magnetic resonance imaging (MRI), single photon emission computed tomography (SPECT) and positron emission tomography (PET), computed tomography (CT) are considered as far better techniques for providing deep tissue information (4) than fluorescence imaging. However, these imaging techniques lack real-time imaging capabilities which would be extremely beneficial during surgery in differentiating malignant from normal tissues and, thereby ensure complete tumor removal (5,6). Intraoperative imaging is not performed with most imaging modalities due to the time of acquisition and data processing/interpretation. A major benefit of fluorescence optical imaging offers the ability for intraoperative imaging or image-guided surgery as image acquisition does not interfere with the treatment process and acquisition/data processing are instantaneous (7). Improved fluorophores for fluorescence optical imaging are now needed and are currently under development.

The sensitivity of fluorescence detection is often limited by autofluorescence of biologic samples. As the extinction wavelength becomes longer the autofluorescence decreases, and hence detectability over background increases. For fluorescence based image-guided surgery development, an ideal fluorophore should be nontoxic, target selective and possess near-infrared (NIR) absorption and fluorescence to easily distinguish the compound from tissue and other endogenous absorbers of light such as water, lipids and hemoglobin (4). These required NIR characteristic limits the use of many dyes that are often used in research such as BODIPY, DAPI, FITC, etc. The two most commonly used classes of NIR fluorophores are the organic dyes and nanoparticles. Organic dyes tend to be more biocompatible and do not use potentially toxic heavy metals such as cadmium, tellurium and selenium that fluorescent quantum dots use (8). Among various NIR organic dye fluorophores, the heterocyclic polymethine dyes (cyanine dyes or CDs) have created enormous interest due to their desirable photophysical properties (long wavelength absorption and fluorescence, large Stokes shift and

*Corresponding author email: ravindra.pandey@roswellpark.org (Ravindra K. Pandey)

high extinction coefficient) (9). The FDA approved heptamethine indocyanine green (ICG) has an extremely high binding affinity to albumin and therefore is used primarily for its diagnostic capability in blood flow and determination of cardiac and hepatic function (10). However, ICG lacks tumor selectivity and therefore has limited utility in clinical oncology (11). Several reports have successfully demonstrated methods to improve the tumor-avid ability of ICG analogs by conjugating them with certain targeting groups such as monoclonal antibodies (12,13), peptides (14,15) and folic acid (16) or formulated into nanoparticles (17,18). These approaches have been effective but it is our belief that a rational drug design and structural activity relationship studies (SAR) could be extremely useful in developing tumor selective fluorophores.

The objective of our study was to prepare a series of CDs and investigate the impact of various substituents in tumor retention, imaging ability and to select a dye with desired multifunctional groups for developing cancer targeted and dual imaging (fluorescence-PET, fluorescence-MRI) agents. For our initial study, the commercially available IR820 was synthesized *via* the Vilsmeier–Haack reaction. The key feature of this particular CD is the presence of a centrally located six member carbocyclic system within the heptamethine chain, which improves the rigidity and the stability of the dye (Fig. 1) (19). In addition, the presence of chloro-, bromo- or iodo groups (halogens) at the meso (or "position-a") position of the dyes allows for several established chemical methods of functionalization, which could lead to improved solubility, target specificity and extended conjugation.

The new compounds were characterized by ^{1}H-NMR and mass spectrometry analyses, and their tumor uptake and imaging abilities were determined using BALB/c mice bearing Colon 26 tumor. To the best of our knowledge, these studies are the first to examine how relatively simple changes to the chemical structure of heptamethine cyanines alters tumor avidity. The SAR that emerged from these studies clearly demonstrate that tumor avidity can be dramatically improved with modest structural modifications.

MATERIALS AND METHODS

Animals. All animals used in experiments were housed and cared for under the strict guidelines of the Institutional Animal Care and Use Committee (IACUC) in the Department of Laboratory and Animal Resources (DLAR) core facility at Roswell Park Cancer Institute (Buffalo, NY). Animals were fed with a standard laboratory diet and water *ad libitum* and monitored daily.

Animals used in this study were BALB/cAnNCr mice obtained from Fredrick National Laboratory (Fredrick, MD). Eight to twelve-weeks old animals were inoculated subcutaneously with 1×10^{6} colon 26 cells on the right shoulder where the fur was removed. When tumors reach measurable dimensions of approximately 4 mm × 4 mm, the mice were injected intravenously with the fluorophore(s) and imaged at regular intervals, and the whole body images were (including tumors) were acquired.

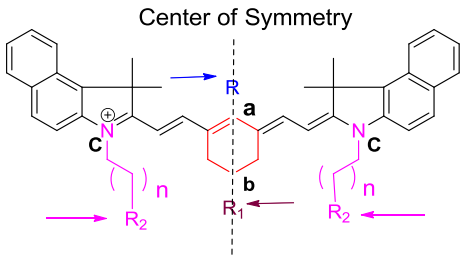

Figure 1. General structure of a NIR cyanine dye.

Drug formulation. 1% Tween 80/D5W. All dyes from this study (with the exception of ICG) were formulated in 1% Tween 80/D5W. Amount of compound and volume of solution were calculated for desired concentration. Final solution was made to be a 1% Tween 80/D5W solution. Compound and necessary volume of tween 80 were added to a mortar and mulled to a paste. The paste was allowed to sit overnight and the next day the calculated amount of D5W was added to the paste and mixed. Solution was filtered through a 0.2 μm syringe filter and concentration was measured spectrophotometrically. Drug formulations were stored at 4°C, when not in use.

Indocyanine green formulation. Stock solution of ICG was made by dissolving ICG powder (Sigma Aldrich, St. Louis, MO) in ddH_2O. The formulation was filtered through a 0.2 μm syringe filter and stored at 4°C. The desired concentration(s) of the dye was obtained by diluting the stock solution with PBS.

Photophysical characterization. UV-visible spectroscopy. UV-Vis absorption spectra of the fluorophores were obtained using a Shimadzu UV-3600 spectrophotometer by diluting drug solutions in methanol to a final concentration of 5 μM. For *in vitro* photobleaching studies, the dyes (5 μM) in methanol were irradiated with 532 nm laser light at 125 mW over time and the fluorescence spectra were recorded using a Fluorolog-3 spectrofluorometer (532 nm excitation, 800 nm and longer emission with 2 nm slit).

Cell culture. All cells were maintained in a humidified incubator at 37°C in atmosphere of 5% CO_2 at 37°C and harvested in log phase of growth at 70–90% confluence.

Murine colon 26 carcinoma cells. Cells were cultured and maintained in sterile RPMI-1640, containing 1× L-glutamine, supplemented with 10% Fetal Calf Serum (FCS) (Atlanta Biologicals, triple 0.1 μm filtered, Lawrenceville, GA) and 1% Penicillin/Steptomycin/L-glutamine (P/S/l-G 10 000 I U mL^{-1} penicillin, 10 000 μg mL^{-1} streptomycin, 29.2 mg mL^{-1} L-glutamine).

ABCG2 expressing HEK-293 482R. Cells were derived in the lab of (late) Dr. Janet Morgan at Roswell Park Cancer Institute, Buffalo, NY and cultured in DMEM supplemented with 10% FCS, 2 mM l-glutamine, penicillin (10 IU mL^{-1}), streptomycin (10 μg mL^{-1}), 2 mg mL^{-1} G418 sulfate (Mediatech, Inc. Manassas VA).

ABCG2 efflux activity assay. HEK-293 cells cultured in selection media were harvested with trypsin, filtered through 30 μm mesh and seeded at low density (400 000 cells) in 5 mL sterile polystyrene tubes. Samples were either blocked with the 10 μM ABCG2 inhibitor Imatinib mesylate (Novartis Pharmaceuticals, Basel Switzerland) or vehicle for 30 min. All samples were performed in triplicate. Samples were then incubated with 0.5 μM cyanine dye for 4 h at 37°C. Previously validated ABCG2 substrate dye N-butyl-O-butyl-bacteriopurpurin was used a positive control. Tubes were placed on ice to inhibit any further × dependent efflux activity and immediately analyzed by flow cytometry (Ex. 785 Em. 830 LP).

In vivo *fluorescence optical imaging*. For all imaging experiments, three mice per drug were injected i.v. with final concentration of each dye was 0.3 μmol k^{-1} body weight of the mice.

Maestro GNIR FLEX. For the CDs **9**–**10** and **14**–**19**, *in vivo* imaging was carried out using the Maestro GNIR FLEX (Cri Inc. Woburn, MA) spectral imaging system. Mice were anesthetized by inhalation of isoflurane (2% in oxygen) and fluorescence spectral cubes were acquired using NIR (illumination light from 780 nm to 950 nm in 10 nm steps at 2 s exposure for each step Ex. 710 nm to 760 nm, Emission 800 nm long-pass) preset filter combinations. Unmixed images, in which background signals were subtracted and quantified by using, built in Maestro software. ROIs (region of interests) were manually selected over various sites over mice and average signal was analyzed.

Nuance camera. Imaging for CDs **17**, **21**, **23** and **25** was performed using a 12 bit Nuance camera (CRI, Worburn, MA) imaging system. Mice were anesthetized by i.p. injection of ketamine/xylene mixture (100/10 mg kg^{-1}) and images were acquired for 5 s with excitation 782 nm emission 800/830 nm long-pass filters over various time points.

IVIS spectrum. Epi-fluorescence imaging of CD **16** and ICG was carried out using the IVIS Spectrum (Perkin-Elmer Waltham, MA) imaging system. Mice were anesthetized by inhalation of isoflurane (2% in oxygen) and fluorescence images were obtained using the Ex. 745 ± 15 nm, Em. Of 840 ± 10 nm filter combination. The Living Image software

(Perkin-Elmer Waltham, MA) was used to process data. Circular regions of interest (ROI) were defined around the tumor and fluorescent intensity was recorded as the average radiant efficiency ((p s^{-1} cm^{-2} sr^{-1})/(μW cm^{-2})).

Postacquisition image processing. Maestro and Nuance Camera unmixed images were processed using ImageJ 1.44p (NIH) software. Grayscale images were enhanced using Lookup Tables setting Royal and brightness was adjusted using Image Adjust setting of Brightness/Contrast. All images shown were set to different scales.

Statistical analysis. All data were analyzed using Graph Pad Prism 5 software (GraphPad Software, San Diego, CA). To test for differences between two groups with normal distribution, a two-tailed Student's *t*-test (unpaired) was used, error bars represent ± standard deviation of mean, the confidence intervals set at 95%.

Chemistry. All reactions were carried under an inert atmosphere using heat gun dried glassware. The reaction mixture(s) was stirred using a magnetic stirrer. Thin-layer chromatography (TLC) was done on precoated silica gel sheets (layer thickness: 0.25 mm) or aluminum oxide sheets. Column chromatography was performed either over silica gel 60 (70–230 mesh) or neutral alumina grade III. In some cases preparative TLC was used for the purification of compounds. Solvents were dried following the standard methodology. ^{1}H NMR spectra were recorded at room temperature in $CDCl_3$ solution using a Varian VNMRS-400 spectrometer. All chemicals shifts are reported in parts per million (δ). ^{1}H NMR (400 MHz) spectra were referenced to residual $CHCl_3$ (7.26 ppm) or TMS (0.00 ppm). Mass spectrometry analyses were performed at the Mass Spectrometry Facility, Michigan State University, East Lansing. UV-visible spectra were recorded on FT UV-visible spectrophotometer using dichloromethane/THF as solvent.

General procedure for the synthesis of NIR cyanine dyes. Commercially available CD **9** (IR820) was purchased from Sigma Aldrich, St. Louis, MO, while the CDs **10**, **15** and **16** were prepared according to the published procedure (20–22). In general, the overall synthesis of cyanine dyes involves three main steps (2.9.1–2.9.3) and was carried out using modified reported procedure (23).

***Step-1*:** A solution of *N, N*-Dimethyl formamide (1 mmole) in dichloromethane (10 mL) was stirred at 0°C and was added phosphorus oxychloride (1 mmole) drop wise over a period of 15 min. After stirring for an additional hour at 0°C, cyclohexanone (**1**–**3**) derivative (2 mmole) was added to the reaction vessel. The entire mixture was heated under reflux for 1 h, then cooled and treated with a mixture of aniline and ethanol (1:1). For **7**, *N,N*-Dimethyl formamide was used instead of the combination of aniline and ethanol. Stirring was continued for an additional 30 min, and then the resulting solution was poured onto a mixture of crushed ice and concentrated hydrochloric acid. The crude mixture was kept at 4°C for overnight; the resulting crystalline product was filtered. The precipitate was washed with cold water and ether, and finally dried under a reduced pressure; yielded the corresponding cyclohexene analogs **4**–**7** in >60% yield.

***Step-2*:** Indolium salt **8** (2 mmol), Vilsmeier–Haack reagent (1 mmol) and anhydrous sodium acetate (4 mmol) were dissolved in absolute ethanol (25 mL) and the entire mixture was stirred at room temperature for 12 h under a nitrogen atmosphere. The intermediate **7** showed limited solubility in ethanol, and therefore, *N, N*-dimethylformamide was used as a solvent. The residue obtained after removing the solvent on a rotary evaporator, was treated with ether (drop by drop). The product so obtained was filtered, and the crude dye was further purified by Silica Gel column chromatography, eluting with dichloromethane/methanol (90:10) to afford the pure cyanine dye(s) **9**–**12** in modest yield (40–55%).

Step-3: A solution of cyanine dye (1 mmol) and thiophenol derivative (10 mmol) in anhydrous *N,N*-dimethylformamide (20 mL) under a nitrogen atmosphere was stirred at room temperature for 12 h. The solvent was removed on a rotary evaporator and the crude obtained was triturated with diethyl ether to precipitate the thiol substituted cyanine dye, which was further purified by silica gel chromatography, eluting with dichloromethane/methanol (90:10) to obtain the pure dye (s) **14**–**19** in the range 60–80% yield.

***Step 4*:** (Used only for the preparation of CD **21**): To a dry flask, the dye **10** (1.0 mmol), 4-carboxyphenylboric acid (**20**) (1.8 mmol) and degassed water (10 mL) was added. The reaction mixture was heated under reflux in the presence of $Pd(PPh_3)_4$ (0.065 mmol) for 12 h. The reaction progress was monitored by visible/near-infrared spectroscopy for aliquots diluted with methanol until absorption of the starting chloro cyanine disappears. The reaction mixture was then cooled to room temperature. The reaction product obtained after removing the water (under vacuum) was suspended in ether, and the product was filtered and was further purified by silica gel column chromatography (10% MeOH-DCM) to afford the desired CD **21**.

Synthesis of the cyanine dye 11. The synthetic steps 1 and 2 as discussed above were followed by reacting compound **5** (obtained from cyclohexanone **3**) with benzoindolium salt **8**, and the title compound was isolated in 46% yield after following the standard procedure. UV-vis λ_{max} (in MeOH): 820 nm; ^{1}HNMR (400 MHz, CD_3OD): δ 8.60 (d, 2H, J = 14 Hz), 8.26 (d, 2H, J = 10 Hz), 7.99 (m, 4H), 7.62–7.69 (m, 5H), 7.49 (t, 2H, J = 7.2 Hz), 7.32 (t, 2H, J = 7.2 Hz), 7.10 (m, 1H), 6.43 (d, 2H, J = 14 Hz), 4.35 (t, 4H, J = 7.6 Hz), 3.22 (dd, 1H, J = 4, 12 Hz), 2.82–3.00 (m, 8H), 1.87–2.15 (m, 22H),. EIMS (*m/z*): 991 (M^+ +2Na). HRMS: Calcd. For $C_{53}H_{56}ClN_3O_7S$: 945.3248. Found: 945.3276.

Synthesis of cyanine dye 12. The cyclohexanone **3** was converted to the corresponding intermediate **7**, by following the general procedure (step 1). It was dissolved in N, N-dimethyl formamide and reacted with benzoindolinium salt **8** to afford the title compound in 42% yield. UV-vis λ_{max} (in MeOH): 820 nm, ^{1}HNMR (400 MHz, CD_3OD): δ 8.55 (d, 2H, J = 14 Hz), 8.26 (d, 2H, J = 8.4 Hz), 8.02 (d, 2H, J = 10.8 Hz), 7.98 (d, 2H, J = 8.4 Hz), 7.79 (d, 2H, J = 9.2 Hz), 7.63 (dt, 2H, J = 8.4, 1.2 Hz), 7.48 (dt, 2H, J = 7.6, 0.8 Hz), 6.41 (d, 2H, J = 14 Hz), 4.37 (t, 4H, J = 7.2 Hz), 3.15–3.18 (m, 2H), 2.90 (t, 4H, J = 7.6 Hz), 2.67–2.76 (m, 3H), 2.08–2.12 (m, 4H), 2.03 (s, 12H), 1.96–2.00 (m, 4H),. EIMS (*m/z*): 915 (M^+ +2Na); HRMS: Calcd. For $C_{47}H_{50}N_2O_8S_2Cl$: 869.2697. Found: 869.2659.

Synthesis of cyanine dye 14. It was prepared by reacting **9** with thiophenol **13** following the general procedure discussed above (step 3) in 78% yield. UV-vis λ_{max} (in MeOH): 831 nm ($\in$ = 157 000 cm^{-1}); ^{1}HNMR (400 MHz, CD_3OD): δ 8.90 (d, 2H, J = 14 Hz), 8.14 (d, 2H, J = 10 Hz), 7.95 (t, 4H, J = 10 Hz), 7.56–7.64 (m, 5H), 7.44 (t, 2H, J = 7.2 Hz), 7.33 (m, 3H), 7.10 (m, 1H), 6.36 (d, 2H, J = 14 Hz), 4.29 (t, 4H, J = 7.6 Hz), 2.84–2.94 (m, 8H), 1.97–2.15 (m, 10H), 1.79 (s, 12H). EIMS (*m/z*): 946 (M^+ +2Na); HRMS: Calcd. For $C_{52}H_{56}N_2O_6S_3$: 901.3379. Found: 900.3362.

Synthesis of cyanine dye 17. Compounds **10** with **13** (4-aminophenylthiol) were reacted by following the methodology as discussed above (step 3) and the title compound was obtained in 73% yield; UV-vis λ_{max} (in MeOH): 829 nm, ^{1}HNMR (400 MHz, CD_3OD): δ 9.00 (d, 2H, J = 14 Hz), 8.22 (d, 2H, J = 14 Hz), 7.91–8.02 (m, 4H), 7.58–7.63 (m, 4H), 7.44 (t, 2H, J = 7.2 Hz), 7.10 (d, 2H, J = 8.4 Hz), 6.62 7.10 (d, 2H, J = 8.4 Hz), 6.38 (d, 2H, J = 14 Hz), 4.34 (t, 4H, J = 7.6 Hz), 4.22 (q, 2H, J = 8.0 Hz), 2.82–2.94 (m, 2H), 1.95–2.08 (m, 10H), 1.85 & 1.82 (s, 12H), 1.24 (t, 3H, J = 7.2 Hz). EIMS (*m/z*): 1032 (M^+ +2Na); HRMS: Calcd. For $C_{55}H_{61}N_3O_8S_3$: 987.3621. Found: 987.3570.

Synthesis of cyanine dye 18. Synthesized by following the procedure discussed above (step 3) by reacting dye **11** with **13** (4-aminophenylthiol) in 77% yield; UV-vis λ_{max} (in MeOH): 825 nm, ^{1}HNMR (400 MHz, CD_3OD): δ 9.02 (d, 2H, J = 14 Hz), 8.18 (d, 2H, J = 8.4 Hz), 8.02 (d, 2H, J = 10.8 Hz), 7.97 (t, 2H, J = 8.4 Hz), 7.67 (d, 2H, J = 9.2 Hz), 7.60–7.63 (m, 4H), 7.48 (dt, 2H, J = 7.6, 0.8 Hz), 7.32 (t, 2H, J = 7.6 Hz), 7.14 (d, 2H, J = 8.8 Hz), 6.68 (d, 2H, J = 8.8 Hz), 6.39 (d, 2H, J = 14 Hz), 4.29 (t, 4H, J = 7.2 Hz), 3.15–3.21 (m, 2H), 2.80–2.96 (m, 3H), 2.85 (t, 4H, J = 7.6 Hz), 1.92–2.12 (m, 4H), 1.98 (s, 6H), 1.83 (s, 6H).. EIMS (*m/z*): 1079 (M^+ +2Na); HRMS: Calcd. For $C_{59}H_{62}N_4O_7S_3$: 1034.3781. Found: 1034.3770.

Synthesis of cyanine dye 19. The desired dye was obtained by reacting **12** with **13** (4-aminophenylthiol) in 80% yield (for a general procedure, see step 3). UV-vis λ_{max} (in MeOH): 825 nm, ^{1}HNMR (400 MHz, CD_3OD): δ 8.43 (d, 2H, J = 14 Hz), 8.15 (d, 2H, J = 8.4 Hz), 7.92 (d, 2H, J = 8.8 Hz), 7.88 (d, 2H, J = 10.8 Hz), 7.59 (d, 2H, J = 8.8 Hz), 7.53 (dt, 2H, J = 8.4, 1.2 Hz), 7.37 (dt, 2H, J = 7.6, 0.8 Hz), 6.91 (d, 2H, J = 8.4 Hz), 6.55 (d, 2H, J = 9.2 Hz), 6.31 (d, 2H, J = 14 Hz), 4.26 (t, 4H, J = 7.0 Hz), 3.13–3.17 (m, 2H), 2.82 (t, 4H, J = 7.6 Hz), 2.55–2.63 (m, 3H), 1.86–2.02 (m, 8H), 1.92 (s, 12H).. EIMS (*m/z*): 915 (M^+ +2Na); HRMS: Calcd. For $C_{53}H_{58}N_3O_8S_3$: 960.3381. Found: 960.3410.

Synthesis of cyanine dye 21. Following the methodology presented above (step 4), the CD **10** and 4-aminoboronic acid **20** were reacted and the title CD was obtained in 48% yield; UV-vis λ_{max} (in MeOH): 787 nm, ^{1}HNMR (400 MHz, $CDCl_3$): 8.07 (d, 2H, J = 8.0 Hz), 7.94 (t, 4H, J = 8.0 Hz), 7.53–7.61 (m, 6H), 7.40–7.44 (m, 2H), 6.98–7.01 (m, 4H), 6.23 (d, 2H, J = 12 Hz), 4.21–4.27 (t, 6H), 3.02–3.05 (m, 4H),

2.86–2.92 (m, 6H), 1.90–2.03 (m, 10H),1.59 (s, 12H), 1.27–1.32 (m, 3H). EIMS (*m/z*): 1000 (M^+ +2Na); HRMS: Calcd. For $C_{55}H_{62}N_3O_8S_2$ (M^+ 2): 956.3973. Found: 956.4007.

Synthesis of cyanine dye 23. By following the procedure discussed in step 1, compound **2** was first converted to **6**, which on reacting with **22** (step 2)**,** gave the title compound in 51% yield; UV-vis λ_{max} (in MeOH): 816 nm; ^{1}HNMR (400 MHz, $CDCl_3$): δ 8.52 (d, 2H, J = 14 Hz), 8.23 (d, 2H, J = 8.8 Hz), 7.95–8.0 (m, 4H), 7.68 (d, 2H, J = 8.8 Hz), 7.61 (t, 2H, J = 7.2 Hz), 7.46 (t, 2H, J = 7.2 Hz), 6.41 (d, 2H, J = 14 Hz), 4.52 (t, 4H, J = 7.2 Hz), 4.19 (q, 2H, J = 7.2 Hz), 3.28–3.30 (m, 3H), 3.05–3.30 (m,2H), 2.90–2.94 (m, 2H), 2.69 (t, 4H, J = 7.6 Hz),1.99 (s, 12H), 1.27 (t, 3H, J = 7.2 Hz). EIMS (*m/z*): 816 (M^+ 2Na). HRMS: Calcd. For $C_{47}H_{48}N_2O_6Cl$ (M^+ 1): 771.3201. Found: 771.3218.

Synthesis of cyanine dye 25. The cyanine dye **23** was reacted with thiol **24** by following the general procedure discussed above (step 3) and the title compound was isolated in 55% yield; UV-vis λ_{max} (in MeOH): 827 nm; ^{1}HNMR (400 MHz, $CDCl_3$): 8.95 (d, 2H, J = 14.4 Hz), 8.16 (d, 2H, J = 8 Hz), 7.95 (t, 4H, J = 8.0 Hz), 7.56–7.64 (m, 4H), 7.43 (t, 2H, J = 7.2 Hz), 7.08 (d, 2H, J = 8.0 Hz), 6.65 (d, 2H, J = 8.0 Hz), 6.44 (d, 2H, J = 16 Hz), 4.49 (t, 4H), 4.17 (q, 2H, J = 8.0 Hz), 2.97–3.09 (m, 5H), 2.65–2.74 (m, 4H),1.87 & 1.81 (s, 12H), 1.27 (t, 3H, J = 7.2 Hz). EIMS (*m/z*): 905 (M^+ 2Na). HRMS: Calcd. For $C_{53}H_{54}N_3O_6S$ (M^+ 1): 860.3733. Found: 860.3748.

General plate irradiation procedure. A stock solution of **21a** (5 mM DMSO) was diluted in water to a final concentration of 20 μM. Samples in 96-well plates (Corning UV-transparent acrylic copolymer) were irradiated using a 780 nm LED $\pm$ 20 nm (L690-66-60, Marubeni America Co.) at a light intensity of 15 mW cm^{-2} as measured using a power meter. Wells containing 300 μL of the 20 μM solution were irradiated and analyzed at 5 min intervals by single point absorption (825 nm). Experiments were run in duplicate and plotted with error bars derived from the standard deviation (<5% in all cases).

Procedure for LC/MS relative Ion analysis of photolysis of 21a. Leaving the solution of compound **19** containing a –COOH functionality in the central cyclohexene ring in methanol converted it the corresponding methyl ester **21a**. A stock solution of **21a** (5 mM DMSO) was diluted in water to a final concentration of 40 μM. Phenylalanine (40 μM) was used as an internal standard. The photolysis was run for 60 min at rt with 20 mW cm^{-2} 780 nm ($\pm$20 nm) light in a 1.5 mL HPLC vial. At time = 0 (prior to irradiation) and 60 min the samples were analyzed by a direct loop injection method with a Shimadzu LCMS-2020 Single Quadrupole instrument (normal resolution). The relative ion counts were calculated by integrating the extracted ion chromatogram (EIC) of the *m/z* of **21a**, oxindole **26**, analogue **28**, and corresponding carbonyl **27** and **29**, and then dividing by the ion count of the phenylalanine internal standard.

RESULTS

Photophysical properties of NIR cyanine dyes

The photophysical characterizations [absorption, fluorescence and extinction coefficient values (molar absorptivity)] of all the cyanine dyes were performed in methanol. All synthetic dyes reported herein exhibited similar photophysical properties and the results are summarized in Table 1.

The longest wavelength absorptions of all dyes were in a range 788–837 nm. The Stokes shifts (shifts between the absorption and emission wavelengths) were in a range 25 nm (390 cm^{-1}) to 41 nm (565 cm^{-1}) and the extinction coefficient values (molar absorptivity) in methanol were in the range 157 000–226 000 M^{-1} cm^{-1}.

Effects of the presence and position of substituents in *in vivo* efficacy of cyanine dyes: A structure–activity relationship (SAR) study

To determine the *in vivo* tumor selectivity of the series of dyes, time course studies using *in vivo* fluorescence optical imaging were performed. The main objectives of this study were (1) to determine the optimal time of accumulation of the dye within the tumor; (2) to determine clearance of the dye from the tumor with time; (3) to evaluate tumor specificity (*e.g.* uptake in tumor *vs* surrounding tissues tissue, and finally; and (4) to monitor the clearance of the dye from the liver and other organs. For imaging studies, a single filter set was used to capture images. However, due to significant differences in the absorption maxima of the dyes synthesized, and the instrumentation limitations to excite the wavelength at the optimal maxima of each CD, direct comparison of one dye over the other could not be performed. Therefore, analysis for selectivity was based on the relative intensities of the fluorescence signal through the body and more specifically, to those measured in tumor, liver and distal skin. This selectivity was determined by injecting a single dose of 0.3 μmol kg^{-1} compound in groups of 3 BALB/c mice bearing colon 26 tumors and observing uptake at various time points post injection.

Table 1. Photophysical properties of cyanine dyes in equimolar concentrations (solvent: methanol). Extinction coefficients values (molar absorptivity) are presented at the longest wavelength absorption of each dye.

Compound	Abs. (λ_{max}, nm)	Fluor. (λ_{max}, nm)	Stokes shift	Molar absorptivity (M^{-1} cm^{-1})
9	820	854	34 nm or 485 cm^{-1}	184 000
10	816	854	38 nm or 545 cm^{-1}	194 300
14	831	872	41 nm or 565 cm^{-1}	157 000
15	837	876	39 nm or 532 cm^{-1}	197 000
16	830	878	38 nm or 659 cm^{-1}	207 500
17	829	866	37 nm or 515 cm^{-1}	217 800
18	825	864	39 nm or 547 cm^{-1}	226 000
19	835	870	35 nm or 482 cm^{-1}	203 000
21	788	813	25 nm or 390 cm^{-1}	190 000
23	816	852	36 nm or 518 cm^{-1}	175 000
25	827	859	32 nm or 450 cm^{-1}	180 000

To determine the impact of various substituents on the tumor imaging ability of heterocyclic heptamethine dyes, a variety of functionalities were introduced at position-a, position-b (cyclohexene moiety) and position-c (Fig. 1). A known methodology was followed for the preparation of CDs **9** and **10**. Attempts to convert the ethyl ester functionality at position-b of the CD under acidic conditions (under basic conditions, the CD was not stable) produced decomposition products, and the desired analog was isolated in a poor yield. Therefore, we used another strategy and the substituted cyclohexane **2** was reacted with aniline and phosphorous oxychloride ($POCl_3$) in dimethylformamide (DMF), which gave the corresponding Schiff base intermediates (Scheme 1), which on reacting with indolium salt **8**, afforded the desired cyanine dyes **10** and **12** in modest yields. To avoid the formation of side products associated with reacting cyclohexane **3** with aniline, cyclohexane **3** was reacted with $POCl_3$ in DMF to yield the intermediate **7,** which on subsequent reaction with NaOAC in DMF gave CD **12**. To investigate the impact of chloro *vs* phenyl or substituted (-NH_2, -COOH, -H) phenyl groups in tumor uptake, CDs **10–12** were reacted with various aromatic thiols **13** (X = various groups) and a series of substituted CDs were synthesized (Scheme 1).

Effect of substituents at position-a. To understand the importance of chloro (-Cl) group at position-a of CD 9, it was reacted with

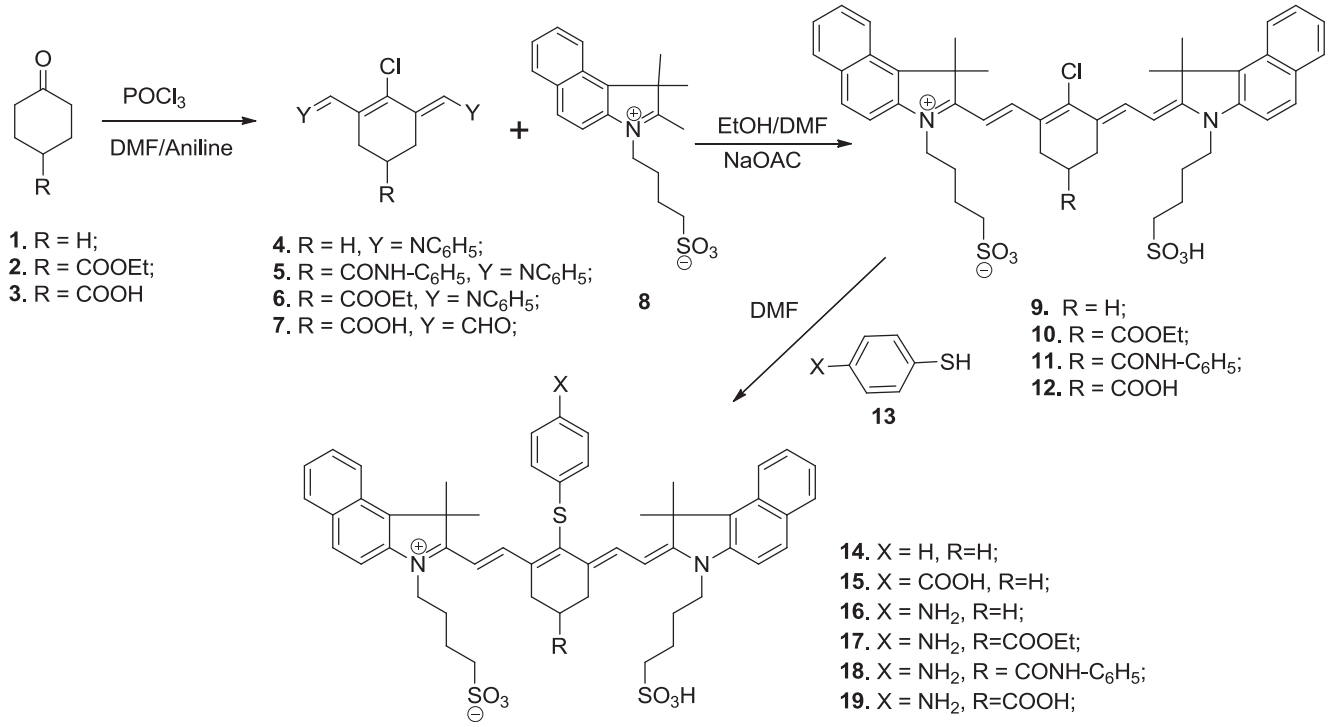

Scheme 1. Synthesis of substituted cyanine dyes bearing N-alkyl sulfonate groups.

phenyl thiol, thio-benzoic acid and *p*-thio-aniline and the respective CDs **14, 15** and **16** were obtained in modest yields.

As seen in Fig. 2, CD **9** displayed limited selectivity toward tumor at 4-96 h post injection with significantly high uptake in liver. Among the three CD **9** derivatives, compound **16** in which the chloro group was replaced by a 4-aminophenylthioether group displayed high tumor selectivity, and retained in tumor at 24, 48, 72 and 96 h post injection. In contrast to tumor, a rapid liver clearance especially at 72 and 96 h post injection was observed. Compound **16** exhibited highest liver accumulation at 4 h post injection and dropped to almost undetectable level in liver at 72 h post injection resulting in excellent contrast between the tumor and the rest of the body.

Replacing the amino (-NH_2) group in CD **16** with a carboxylic acid (-COOH) group to yield CD **15** drastically changed the pharmacokinetic profile of the dye, and under similar imaging parameters, displayed extremely low tumor avidity and a faster clearance from the system.

CD **14** obtained by removing the amino group in CD **16** at position-a showed limited accumulation in tumor and, in contrast produced high uptake and retention in liver for a long time, even at 96 h post injection. *Effect of substituents at position-b:* Position-b modification started with the synthesis of CD 10 (position-a -Cl, position-b ethyl ester) following the method described by Strekowski *et al.* (23). After introducing anethyl ester functionality at position-b of IR820, the compound was reacted with 4-aminophenylthiol and CD 17 was obtained in good yield. Interestingly, compared to CD 16, the addition of the ethyl ester functionality to it (CD 17) reduced its tumor uptake/specificity (Fig. 3). However, compared to the parent CD 10 bearing a Cl^- group at position-a, the 4-aminophenylthioetrher analog 17 did display more favorable tumor localizing ability. The CD 17 appeared to maintain high levels of uptake in the liver at 72 h post injection and therefore, did not provide the same level of tumor to whole body contrast as CD 16. Attemp**ts to hydrolyze the ethyl ester** functionality at position-b of CD 10 to a carboxylic acid had limited success and resulted in decomposition. Under similar reaction conditions, the CD 17 resulted in a loss of the 4-aminophenylthiolether functionality. Therefore, CD 19 (position-a **bearing a** 4-aminophenylthiol, and at position-b **bearing a** carboxylic acid) was prepared *via* a stepwise synthesis (Scheme 1).

The newly synthesized CD analogs were evaluated for tumor–uptake/imaging potential at variable time points under similar imaging dose (0.3 μmol kg^{-1}) in BALB/c mice bearing colon 26 tumors, and the results are illustrated in Fig. 3. In brief, compared to CD **17**, the dye **19** produced similar tumor uptake**,** but showed faster clearance from the liver. This could possibly be attributed due to the change in pharmacokinetic profile of the molecule on introduction a carboxylic acid functionality. Again, the presence of an amino-phenyl group at position-b (CD **18**) showed slightly enhanced tumor uptake.

Importance of a thioether linker at position-a of the CDs investigated. To determine the importance of thioether linker between the 4-aminophenyl and the cyanine dye, CD **10** (position-a -Cl, position-b ethyl ester) was reacted with *p*-aminophenyl boronic acid **20** under Suzuki–Miyaura reaction conditions and the desired compound **21** was isolated in modest yield (Scheme 2). In contrast to other position-a substituted CDs, which resulted in a bathochromic shift, the CD **21,** where the chloro group was substituted with an aminophenyl group (linked with C–C bond) exhibited a hypsochromic shift exhibiting a strong absorption at 788 nm (ε = 190 000).

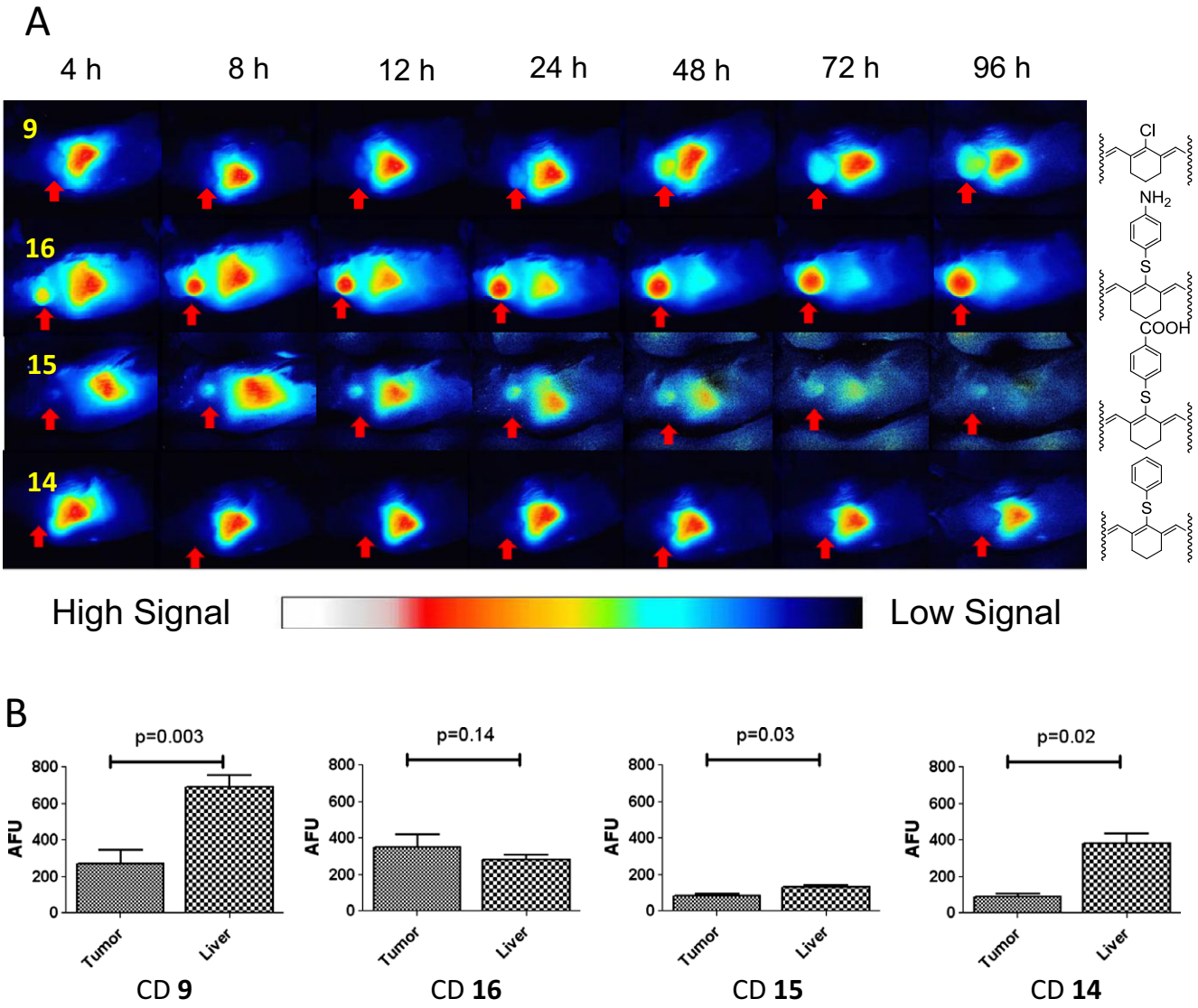

Figure 2. Unscaled whole body imaging of 0.3 μmol kg^{-1} CDs **9**, **14**, **15** and **16** over 96 h in a representative BALB/c mouse with colon 26 tumors. Images acquired using Maestro GNIR Flex NIR filter set (Ex. 710–760 nm, Em. 800 nm long-pass, 2 s exposure) (A) One representative mouse per dye across all time points is depicted. Tumor location is indicated with red arrows and while liver is located just right of tumor. Arbitrary scale bar included for signal reference (B) Average signals from tumor and liver of three mice per group per drug at only the 24 h time point. Maestro software was used to acquire signal level. Error bars represent standard deviation; Student's *t*-test *P* values are shown.

The *in vivo* results summarized in Fig. 4 indicate that similar to CD **17** (containing a sulfur linker), compound **21** (no sulfur linkage) produced higher uptake at 24 to 48 h post injection.

Effect of substituents at position-c. In the most of the symmetrical and nonsymmetrical cyanine dyes, including ICG, in which the sulfonic acid functionalities are attached either at position-c or in aromatic ring system(s) and the dyes generally show enhanced tumor uptake/retention and faster clearance from the rest of the organs. Presence of sulfonic acid groups in CDs seems to improve their water solubility, and also prevents the aggregation of the dyes (24).

To investigate the impact of such substitutions, the tumor uptake and fluorescence imaging potential of CD **17** was compared with CD **25,** in which the sulfonic acid functionalities (-SO_3H) were replaced with carboxylic acid (-COOH) groups. The position-c carboxylic acid derivatives were synthesized by following a similar synthetic approach as discussed for the preparation of CD **10**, in which the benzoindole **22** (instead of **8**) was reacted with Schiff's base **6** (Scheme 3). The resulting intermediate CD **23** was reacted with 4-aminophenylthiol (**24**) to give the desired cyanine dye **25** in 55% yield.

To investigate the difference in tumor specificity of the CDs containing the sulfonic acid *vs* carboxylic acid functionalities, tumor uptake of CD **17** (4-aminophenylthioether group at position-a ethyl ester functionality at position-b, and N-alkyl sulfonate group at position-c), and CD **25** (4-aminophenylthioether group at position-a ethyl ester functionality at position-b, and N-alkyl carboxylic acid group at position-c), was compared in tumored mice (BALB/c mice bearing Colon26 tumors). To Further validate the importance of 4-aminophenylthiol, CD **23** (position-a –Cl, position-b ethyl ester, position-c N-alkyl

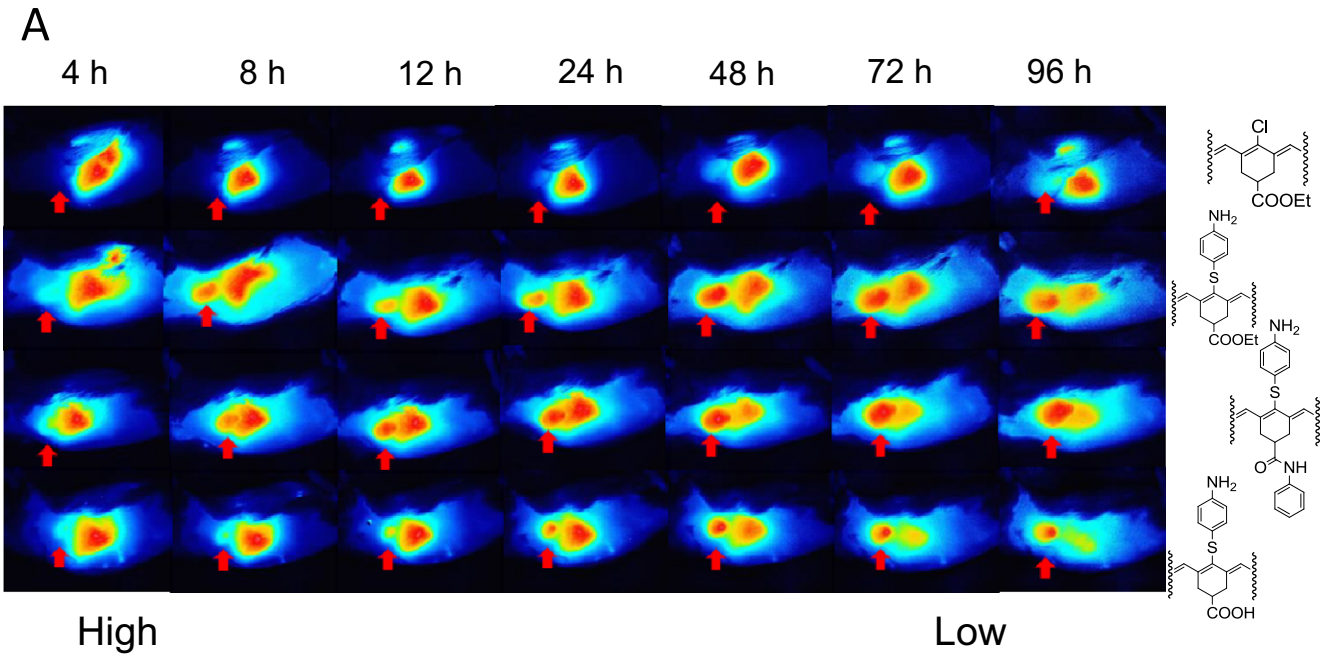

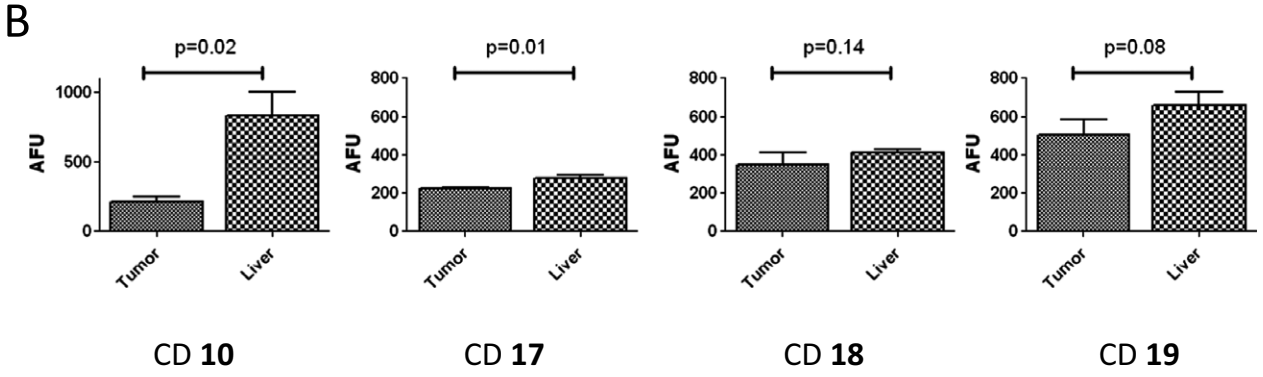

Figure 3. Whole body imaging of BALB/C mice (three mice/group, the image of only 1 mouse/CD is shown) bearing colon 26 tumors injected with CDs **10**, **17**, **18** or **19** (dose: 0. 3 μmol kg^{-1}) over 96 h. Images acquired using Maestro GNIR Flex NIR filter set (Ex. 710–760 nm, Em. 800 nm long-pass, 2 s exposure) (A) One representative mouse per dye across all time points is depicted. Tumor location is indicated with red arrows and while liver is located just right of tumor. Arbitrary scale bar included for signal reference (B). Maestro software was used to acquire average concentration of the dye from tumor *vs* liver (using three mice/group/drug at 24 h post injection). More specifically, using the built in Maestro software, regions of interest (ROI) were drawn over the areas where the tumor and other organs of interest are located. The software subtracted out signals from skin and tissue from a control mouse, and displayed the signal of only the drug within the desired ROI. Error bars represent standard deviation and the Student's *t*-test *P* values are shown.

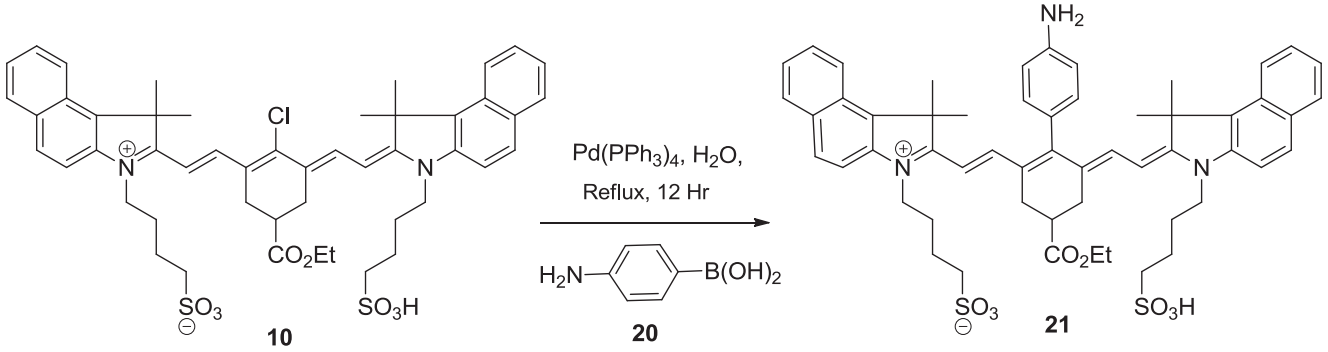

Scheme 2. Synthesis of 4′-aminophenylcyanine dye without thioether linkage.

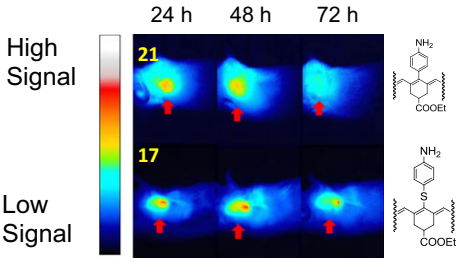

Figure 4. Whole body images of tumor mice showing difference in tumor uptake of CD **17** and CD **21** at 24, 48 and 72 h post injection. One representative BALB/c mouse with colon 26 tumor is shown across multiple time points injected with 0.3 μmol kg^{-1}. Images acquired using Nuance Camera (Ex. 782 nm, Em. 800/830 nm long-pass filters, 5 s exposure). Tumor location is indicated with red arrows. Arbitrary scale bar included for signal reference. Based on the scale from the Image J software, higher signal intensity was observed for compound **17** over **21**.

carboxylic acid) was also included in this study. From the results summarized in Fig. 5, it can be seen that the tumor and liver distribution of CD**17** was far more favorable than CD **25**. CD **17** was rapidly cleared from nontumor sites while CD **25** appeared only to slightly favor tumor accumulation to liver at 24 and 48 h. However, CD **25** displayed much more favorable distribution than CD **23**, again confirming the importance 4-aminophenylthioether group at position-a of the cyanine dye.

Photooxidative reactivity of 21a. Besides the use of CDs in tumor imaging, certain respective targeted or nontargeted CD analogs have also been investigated for their application as photosensitizers for photodynamic therapy (PDT) (25). In our hands, the newly synthesized cyanine dyes, which showed significant potential for tumor imaging produced limited PDT efficacy (not shown) in colon 26 cell lines under the normal PDT treatment parameters (MTT assay), where the required time for light exposure was much longer than used for tumor imaging.

Therefore, determining the stability of cyanine fluorophores under tumor imaging and treatment parameters is extremely important as these methods proceed toward diagnostic and therapeutic applications. Cyanine fluorophores have been reported to undergo oxidative C–C cleavage reactions upon irradiation (26–28). These reactions have been proposed to occur through a mechanism comprising photosensitization to form singlet oxygen, regioselective dioxetane formation and final dioxetane cleavage to form carbonyl products. Using a combination of spectrometry and absorption techniques, it was observed that irradiation of **21a** at 780 nm reduces the near-IR absorbance and leads to the formation of four photooxidative products, **26, 27, 28** and **29** (Fig. 6).

Cyanine dyes specificity toward ABC transport proteins. One of the factors that have been reported to play an important role in the cellular accumulation of many agents including the cyanine dyes is their specificity toward ABC (ATP-binding cassette) transport proteins (29). ABCG2 or breast cancer resistance protein has been found to efflux many classes of compounds used for cancer imaging and therapy. Tyrosine kinase inhibitors (TKI), including imatinib mesylate (Gleevec), are a part of a novel class in cancer treatment which have been found to reverse resistance to chemotherapy drugs and certain photosensitizers by blocking their efflux by ABCG2 (30).

Therefore, our interest was to investigate if the increase in tumor accumulation and retention that occurs by introducing the aminophenylthioether functionality to the CD was the result of pump efflux evasion. Using HEK-293 cells transfected with ABCG2 and NIR flow cytometry we compared the structurally similar CDs **9** (position-a -Cl) and **16** (position-a 4-aminophenylthioether). The *in vitro* results summarized in Fig. 7 indicate that neither dye was a substrate for the ABCG2 dye efflux pump.

Comparative tumor imaging ability of symmetrical cyanine dyes bearing heptamethine linker with and without a fused six member ring in IVIS system. Indocyanine green has extremely high binding affinity to albumin and does not show preferential uptake in tumor cells *versus* normal cells. This partially explains why tumor sites accumulate ICG only for a short time after intra-

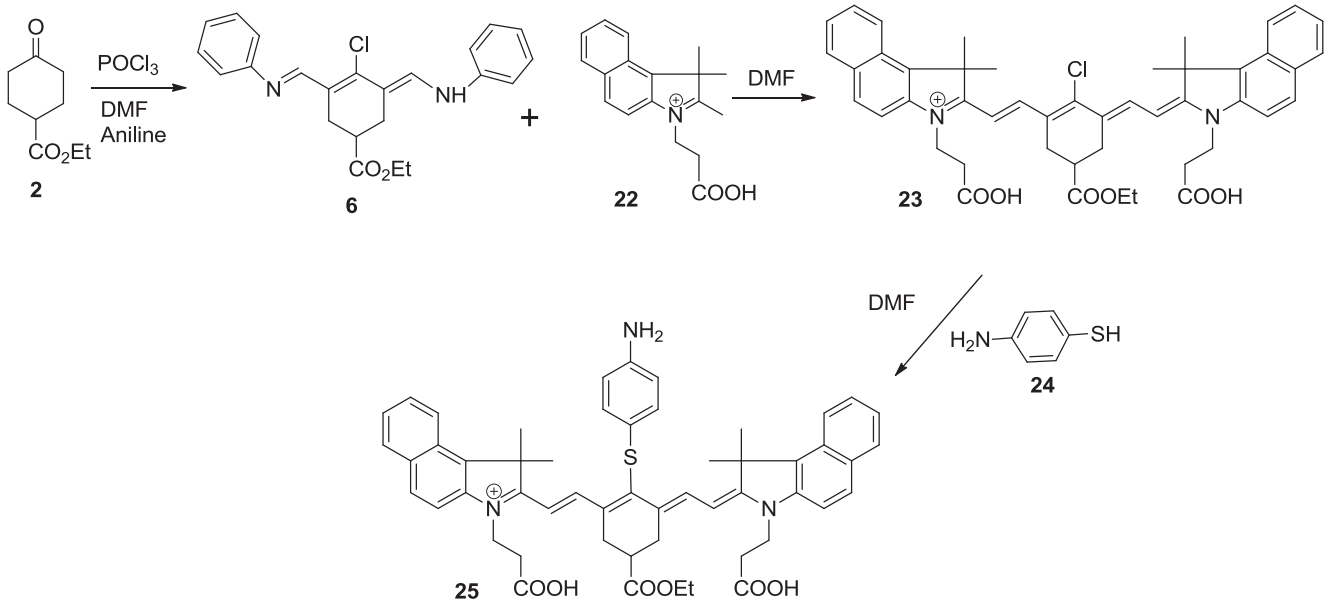

Scheme 3. Synthesis of N-alkyl carboxylic acid containing cyanine dyes.

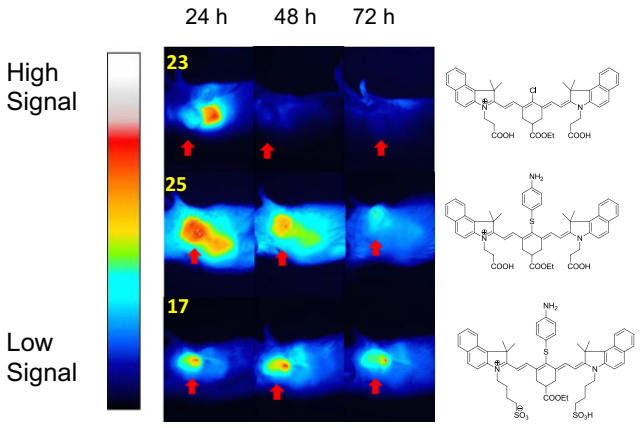

Figure 5. Whole body images of tumored mice showing uptake of CDs **17, 23** and **25** at 24, 48 and 72 h post injection. One representative BALB/c mouse with colon 26 tumor is shown across multiple time points injected with 0.3 μmol kg^{-1}. Images acquired using Nuance Camera (Ex. 782 nm, Em. 800/830 nm long-pass filters, 5 s exposure).Tumor location is indicated with red arrows. Arbitrary scale bar included for signal reference.

venous injection into mice. The leaky and damaged blood vessels of a tumor allow ICG to enter into the tumor and it is quite possible that the cyanine dyes synthesized and investigated in this study are also following a similar pattern. Structurally, ICG does not contain the central fused six member linker which the dyes in our study possess. To gain an understanding of the role of this six member ring, we compared the *in vivo* tumor accumulation of ICG and one of the top candidates (CD **16**) under similar imaging parameters. The *in vivo* results summarized in Fig. 8 illustrate the difference the two compounds in terms of accumulation and pharmacokinetic profile. As can be seen, ICG shows optimal uptake in the tumor at 30 min after injection. However, even at this optimal time of tumor uptake, actual drug localization is limited and ICG is primarily distributed in the digestive system. ICG was found to rapidly clear from the system within 24 h and very little signal above background can be detected. Unlike ICG, CD **16** has very little accumulation in the tumor at 30 min after injection. However, over the course of the experiment this changes greatly. At 48 h post-injection, most of the dye was localized in the tumor, and comparatively low fluorescence throughout the body provided excellent contrast.

DISCUSSION

Recently the work revolving around the use of fluorescent dyes for optical imaging in cancer has proven very promising and has contributed greatly to the adoption of the technology. While current fluorescent dye development is geared toward chemical conjugations of active targeting molecules to confer selectivity, this method has its own limitations. Tumors which do not express these targets would not be detected by these highly selective dye conjugates. In addition, these conjugated dyes such as antibody-dye conjugates tend to be very bulky which limits permeability through membranes and greatly increase the cost of the drug. In

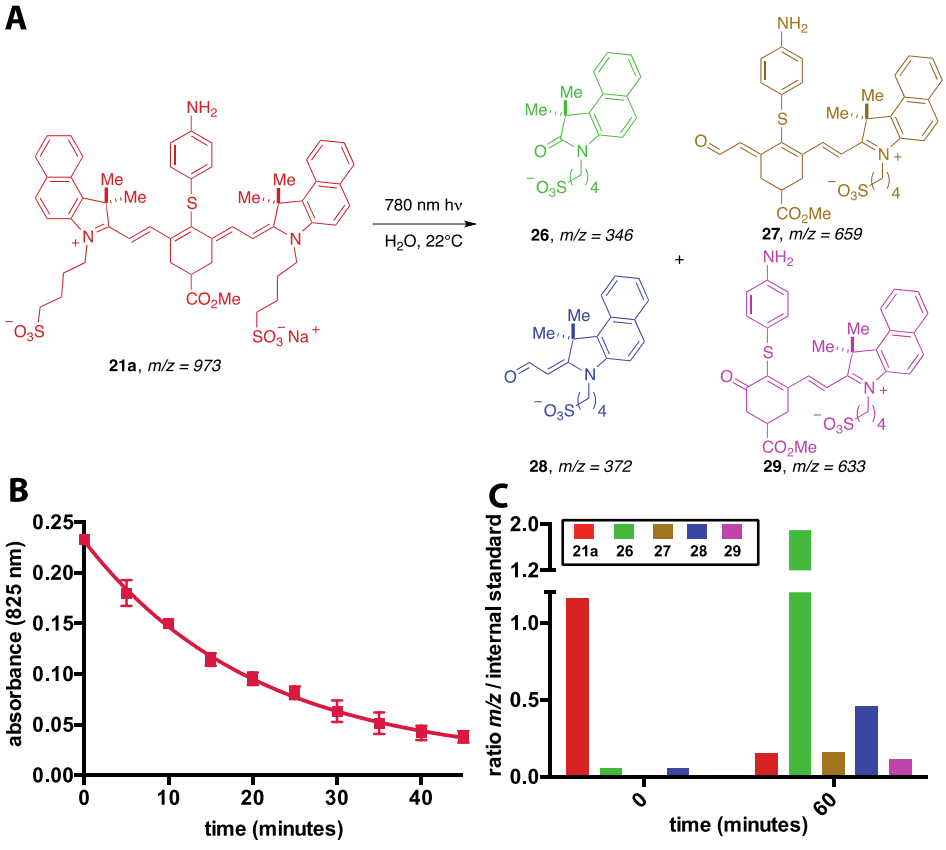

Figure 6. (A) Conversion of **21a** to **26**, **27**, **28** and **29**. (B) Absorption (825 nm) upon exposing a 20 μM solution of **21a** in H_2O to 20 mW cm^{-2} light at rt. (C) Relative spectral ion counts of **26**, **27**, **28** and **29** prior to and after irradiation. Ion counts were determined at each time point relative to an internal standard (phenylalanine).

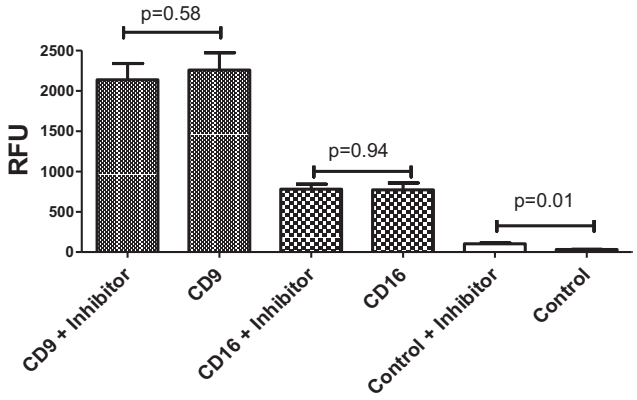

Figure 7. ABCG2 efflux pump susceptibility of dyes with and without pump inhibitor measured by flow cytometry (Ex. 785 Em. 830 LP). 0.5 μmol CD **9**, CD **16** and positive control N-butyl-O-butyl-bacteriopurpurin were incubated for 4 h with and without pump inhibitor Imatinib mesylate. Error bars represent standard deviation. Student's *t*-test *P* values are shown.

this study we have pursued an alternative SAR-driven approach examining the effects of subtle chemical modifications on tumor avidity.

In general, the cyanine dyes tend to have low fluorescence quantum yields, but their inherent high extinction coefficients and reasonable Stokes shifts along with positioning of their absorption/fluorescence in the NIR optical region make them excellent candidates for tumor imaging (31). The *in vitro* photophysical studies of the dyes selected for SAR study demonstrated these dyes possess desirable photophysical properties, e.g. high extinction coefficients of >155 000 M^{-1} cm^{-1}, NIR absorbance maxima >788 nm, fluorescence peaks >813 and Stokes shifts >25 nm.

The lack of availability of an optimal tunable excitation light source and adjustable optical filter sets impedes comparison between the various CD dyes *in vivo* prevents to compare their precise optimal potential. Favorable *in vivo* distribution (tumor accumulation *vs* all other detectable tissue) was used as the screening criteria for the majority of the findings in this study. *In vivo* distribution showed that nucleophilic substitution of the chloro group at position-a of CD **9** has improved selectivity with certain functionalities. Studies on substituting the chloro group with a 4′-thioether (CD **16**) gave the most effective imaging agent. Replacing the amino functionality with a carboxyl group or removing it entirely to form CD **14** and **15,** respectively, resulted in reduced tumor selectivity. Quantification of signal at 24 h post injection showed significantly higher ($P < 0.05$) liver accumulation if compared to tumor for both derivatives while the amino substituted CD **16** was found to have no difference between tumor and liver uptake. This favorable distribution profile of the amino substituted dye was only improved over the time course of this study where the dye was found to be retained in the tumor yet being excreted from the liver thereby providing excellent contrast at later time points. To demonstrate the importance of the sulfur in the 4-aminophenylthioether functionality in CD **16**, CD **21** (with no thioether linkage) was prepared by following Suzuki coupling (32,33). While both compound displayed similar clearance from the liver, CD **21** was found to be less selective as it was shown to linger in the normal tissue around the tumor.

Once the importance of the amino functionality at position-a was validated for enhanced tumor uptake, a synthetic strategy to introduce a variety of substituents at position-b of the amino-phenyl functionalized CD was developed. Compared to position-a modified CD, substituents introduced at position-b did not show such a profound difference in tumor avidity. However, the availability of a facile synthetic approach for introducing desired functional groups at positions-a, -b and -c provides an opportunity to develop a wide variety of bi or multi-imaging (fluorescence/PET, fluorescence/MRI) agents with and without tumor targeting

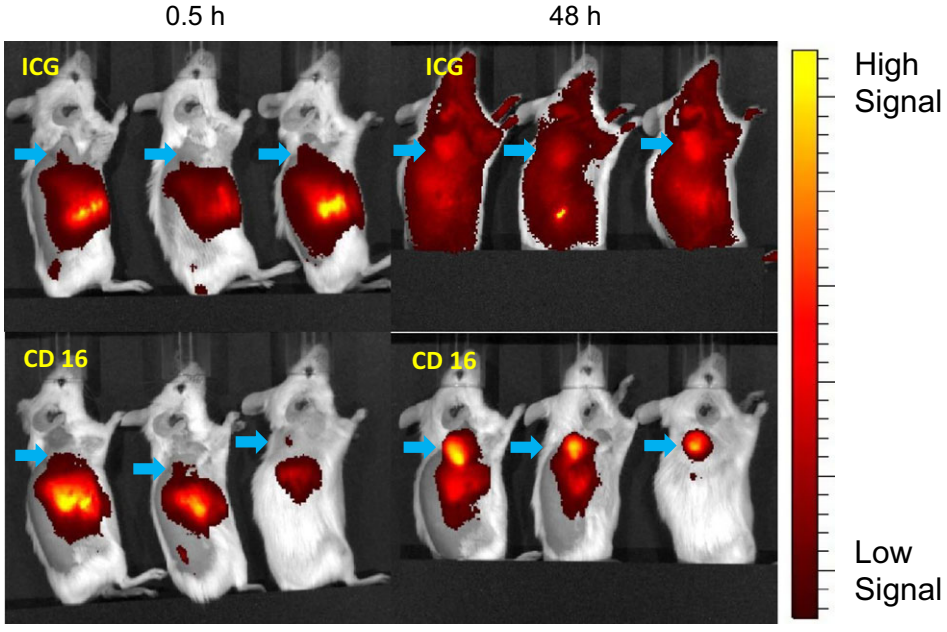

Figure 8. Whole body images of tumored mice (BALB/c mice with colon 26 tumors, three mice/group) injected with ICG and CD**16** at a dose of 0.3 μmol kg^{-1} over 96 h (only 0.5 and 48 h images are shown). The images were acquired using IVIS Spectrum (Ex. 745 $\pm$ 15 nm, Em. 840 $\pm$ 10 nm) Tumor location is indicated with blue arrows. Arbitrary scale bar included for signal reference.

moieties, and these studies are currently in progress. The tumor imaging ability of the most effective cyanine dye (CD**16**) was also compared with ICG, a clinically approved blood pooling agent, which is also being used for fluorescence imaging to tumors, and it clearly demonstrated enhanced tumor specificity with desirable pharmacokinetic profile. ABCG2 efflux pump substrate studies show that all the cyanine dye are the substrates for the pump and no significant difference between the tumor-avid and nontumor-avid dyes was observed. Like many other drugs, one of the reasons for the difference in tumor specificity of some of the CDs could be due to their differences in binding affinity to human serum albumin (HSA). Possibly, the dye with higher binding affinity tends to retain in circulation for a longer period of time and passes through the leaky tumor vessels. The hydrophobic nature of the dye helps it to accumulate, and retain in tumor for a longer period of time than the other organs.

In summary, a series of heterocyclic polymethine dyes were synthesized and characterized and their photophysical properties and *in vivo* tumor localizing/retention ability with time was investigated. Synthetic modifications were made at 3 different positions of heptamethine chain containing a fused chloro-cyclohexene ring system, which allowed us to define, for the first time, key structural features than can improve tumor avidity. For example: (1) replacing the sulfonate groups of N-alkyl sulfonate side chains with carboxylic acid functionalities reduced the tumor uptake significantly; (2) substituting the chloro group in chloro-cyclohexene moiety of the CD with 4-aminophenyl-thioether functionality significantly increased the tumor uptake; and (3) a methodology to introduce carboxylic acid functionality in cyclohexene ring system was established, which provides an opportunity to develop multi-imaging agents. Efforts are currently underway in our laboratory to explore the utility of this approach in developing tumor specific fluorescence/PET, fluorescence/SPECT and fluorescence/MRI dual imaging agents.

Acknowledgements—The financial support from the NIH (CA55791, CA127369 and Photolitec, LLC is gratefully acknowledged. A partial support from the shared resources of the RPCI support grant (P30CA16056) is also appreciated. This work was also supported in part by the Intramural Research Program of the National Cancer Institute, National Institutes of Health. Nayan Patel is thankful to the Department of Molecular Pharmacology and Cancer Therapeutics for providing fellowship from the NIH funded graduate students research training grant.

REFERENCES

1. Zhang, S., N. Patel and R. K. Pandey (2014) Chlorophyll-a analogs for cancer imaging and therapy (theranostics). *Top. Heterocyclic Chem*, **34**, 1–30.
2. Stuker, F., J. Ripoll and M. Rudin (2011) Fluorescence molecular tomography: Principles and potential for pharmaceutical research. *Pharmaceutics* **3**(2), 229–274.
3. Konig, K. (2000) Multiphoton microscopy in life sciences. *J. Microsc.* **2000**, 83–104.
4. Willmann, J. K., N. van Bruggen, L. M. Dinkelborg and S. S. Gambhir (2008) Molecular imaging in drug development. *Nat. Rev. Drug Discov.* **7**(7), 591–607.
5. Eljamel, S. (2010) Photodynamic applications in brain tumors: A comprehensive review of the literature. *Photodiagnosis Photodyn Ther.* **7**(2), 76–85.
6. Eljamel, S., M. Petersan, V. Ronan, B. Ron, C. Goodman, H. Moseley and S. Eljamel (2013) Comparison of intraoperative fluorescence and MRI image guided neuronavigation in malignant brain tumours, a prospective controlled study. *Photodiagnosis Photodyn Ther.* **10** (4), 356–361.
7. Mieog, J. S., M. Hutterman, J. R. van der Vorst, P. J. K. Kuppen, I. Que, J. Dijkstra, E. L. Kaizel, F. Prins, C. W. G. M. Lowik, V. T. H. B. Smit, C. J. H. van de Velde and A. L. Vahrmeijer (2011) Image-guided tumor resection using real-time near-infrared fluorescence in a syngeneic rat model of primary breast cancer. *Breast Cancer Res. Treat.* **128**(3), 679–689.
8. Rizvi, S. B., S. Rouhi, S. Taniguchi, S. Y. Yang, M. Green, M. Keshtgar and A. M. Seifalian (2014) Near-infrared quantum dots for HER2 localization and imaging of cancer cells. *Int. J. Nanomedicine.* **9**, 1323–1337.
9. Nikolova, K., S. Kaloyanova, N. Mihaylova, S. Stoitsova, S. Chausheva, A. Vasilev, N. Lesev, P. Dimitrova, T. Deligeorgiev and A. Tchorbanov (2013) New fluorogenic dyes for analysis of cellular processes by flow cytometry and confocal microscopy. *J. Photochem. Photobiol., B* **129**, 125–134.
10. Murahari, M. S. and M. C. Yergeri (2013) Identification and usage of fluorescent probes as nanoparticle contrast agents in detecting cancer. *Curr. Pharm. Des.* **19**(25), 4622–4640.
11. Licha, K., B. Riefke, V. Ntziachristos, A. Becker, B. Chance and W. Semmler (2000) *Hydrophilic cyanine* dyes as contrast agents for near-infrared tumor imaging: Synthesis, photophysical properties and spectroscopic in vivo characterization. *Photochem. Photobiol.* **72**(3), 392–398.
12. Sano, K., M. Mitsunaga, T. Nakajima, P. L. Choyke and H. Kobayashi (2012) In vivo breast cancer characterization imaging using two monoclonal antibodies activatably labeled with near infrared fluorophores. *Breast Cancer Res.* **14**(2), R61.
13. Sano, K., T. Nakajima, K. Miyazaki, Y. Ohuchi, T. Ikegami, L. P. Choyke and H. Kobayashi (2013) Short PEG-linkers improve the performance of targeted, activatable monoclonal antibody-indocyanine green optical imaging probes. *Bioconjug. Chem.* **24**(5), 811–816.
14. Cao, J., S. Wan, J. Tian, S. Li, D. Deng, Z. Qian and Y. Gu (2012) Fast clearing RGD-based near-infrared fluorescent probes for in vivo tumor diagnosis. *Contrast Media Mol. Imaging* **7**(4), 390–402.
15. Leung, K. (2004) *Indocyanine Green Derivative 02-Glu-c(RGDyK)2, in Molecular Imaging and Contrast Agent Database (MICAD)*. National Center for Biotechnology Information (US), Bethesda, MD.
16. Ma, Y., M. Sadoqi and J. Shao (2012) Biodistribution of indocyanine green-loaded nanoparticles with surface modifications of PEG and folic acid. *Int. J. Pharm.* **436**(1–2), 25–31.
17. Wu, L., S. Fang, S. Shi, J. Deng, B. Liu and L. Cai (2013) Hybrid polypeptide micelles loading indocyanine green for tumor imaging and photothermal effect study. *Biomacromolecules* **14**(9), 3027–3033.
18. Zheng, C., M. Zheng, P. Gong, D. Jia, P. Zhang, B. Shi, Z. Sheng, Y. Ma and L. Cai (2012) Indocyanine green-loaded biodegradable tumor targeting nanoprobes for in vitro and in vivo imaging. *Biomaterials* **33**(22), 5603–5609.
19. Strekowski, L. (2008) *Heterocyclic Polymethine Dyes: Synthesis, Properties and Applications*. Springer, Berlin, Heidelberg.
20. Williams, M. P. A., M. Ethirajan, K. Ohkubo, P. Chen, P. Pera, J. Morgan, W. H. White, M. Shibata, S. Fukuzumi, K. M. Kadish, R. K. Pandey *et al.*, (2011) Synthesis, photophysical, electrochemical, tumor-imaging, and phototherapeutic properties of purpurinimide-N-substituted cyanine dyes joined with variable lengths of linkers. *Bioconjug. Chem.* **22**(11), 2283–2295.
21. Chen, Y., A. Gryshuk, S. Achilefu, T. Ohulchanskyy, W. Potter, T. Zhong, J. Morgan, B. Chance, P. N. Prasad, B. W. Henderson, A. Oseroff and R. K. Pandey (2005) A novel approach to a bifunctional photosensitizer for tumor imaging and phototherapy. *Bioconjug. Chem.* **16**(5), 1264–1274.
22. Strekowski, L., J. C. Mason, H. Lee, H. M. Say and G. Patonay (2004) Water-soluble pH-sensitive 2,6-bis(substituted ethylidene)-cyclohexanone/hydroxy cyanine dyes that absorb in the visible/near-infrared regions. *J. Heterocycl. Chem.* **41**(2), 227–232.
23. Strekowski, L., C. J. Mason, H. Lee, R. Gupta, J. Sowell and G. Patonay (2003) Synthesis of water-soluble near-infrared cyanine dyes functionalized with [(succinimido)oxy]carbonyl group. *J. Heterocycl. Chem.* **40**(5), 913–916.
24. Terpetschnig, E., H. Szmacinski, A. Ozinskas and J. R. Lakowicz (1994) Synthesis of squaraine-N-hydroxysuccinimide esters and their

biological application as long-wavelength fluorescent labels. *Anal. Biochem.* **217**(2), 197–204.
25. Pandey, R. K., N. James, Y. Chen and M. P. Dobhal (2008) Cyanine dye-based compounds for tumor-imaging with and without photodynamic therapy. *Top Heterocyclic Chem.* **14**, 41–74. and references therein.
26. Byers, G. W., S. Gross and P. M. Henrichs (1976) Direct and sensitized photooxidation of cyanine dyes. *Photochem. Photobiol.* **23**(1), 37–43.
27. Engel, E., S. Rudiger, T. Maisch, K. Kobuch, B. Konig, R.-M. Szimies, J. Hillenkamp, W. Baumler and R. Vasold (2008) Light-induced decomposition of indocyanine green. *Invest. Ophthalmol. Vis. Sci.* **49**(5), 1777–1783.
28. Gorka, A. P., R. R. Nani, J. Zhu, S. Mackem and M. J. Schnermann (2014) A near-IR uncaging strategy based on cyanine photochemistry. *J. Am. Chem. Soc.* **136**(40), 14153–14159.
29. Gottesman, M. M., T. Fojo and S. E. Bates (2002) Multidrug resistance in cancer: Role of ATP-dependent transporters. *Nat. Rev. Cancer* **2**, 48–58.
30. Liu, W., M. R. Baer, M. J. Bowman, P. Paera, X. Zgeng, J. Morgan, R. K. Pandey and A. R. Oseroff (2007) The tyrosine kinase inhibitor imatinib mesylate enhances the efficacy of photodynamic therapy by inhibiting ABCG2. *Clin. Cancer Res.* **13**(8), 2463–2470.
31. Fabian, J., H. Nakazumi and M. Matsuoka (1992) Near-infrared absorbing dyes. *Chem. Rev.* **92**(6), 1197–1226.
32. Lee, H., J. C. Mason and S. Achilefu (2006) Heptamethine cyanine dyes with a robust C-C bond at the central position of the chromophore. *J. Org. Chem.* **71**, 7862–7865.
33. Zhang, Z. and S. Achilefu (2005) Synthesis and evaluation of polyhydroxylated naer-infrared carbocyanine molecular probes. *Org. Lett.* **6**(12), 2067–2070.